RSC Advances

PAPER

View Article Online
View Journal | View Issue

Cite this: *RSC Adv.*, 2026, **16**, 20330

Discovery of thieno[3,2-*c*]pyran-based leads for liver, lung and glioma cancer: synthesis, docking-guided optimization and apoptotic profiling

Abhishek Jauhari,[a] Pooja,[b] Lakshay Taneja,[c] Ajay Kumar Yadav,[c] Ismail Althagafi,[d] Ramendra Pratap *[e] and Dharmendra Kumar Yadav *[f]

Thieno[3,2-*c*]pyran is a versatile heterocyclic framework recognised as a core scaffold in numerous synthetic anticancer agents and naturally occurring alkaloids exhibiting potent antitumor activity across various malignancies, including lung, liver, breast, and prostate cancers. In this study, we report the synthesis of a series of substituted thieno[3,2-*c*]pyran derivatives and their biological evaluation against human hepatocellular carcinoma (HepG2) and lung adenocarcinoma (A549) cell lines. The *in vitro* cytotoxicity assays revealed promising IC_{50} values: **5a** exhibited 13.65 ± 0.32 μM (HepG2) and 12.35 ± 0.30 μM (A549), while **5n** showed 13.26 ± 0.32 μM (HepG2) and 12.36 ± 0.30 μM (A549). Apoptosis-induction studies confirmed the anticancer potential of these compounds. However, compound **5e** works well against Glioma cancer with a promising IC_{50} value of 26 μM (LN229). We have also performed the testing of selected compounds against the non-cancerous cell line HEK293 under the same conditions and concentration, and no cytotoxicity. Among the synthesized compounds, **5a** and **5n** demonstrated significant binding affinities in molecular docking studies, with docking scores of −8.834 and −8.994 kcal mol^{-1} against liver cancer targets, and −7.925 and −7.871 kcal mol^{-1} against lung cancer targets, respectively. To further confirm the EGFR inhibition, selected compounds were tested agaist EGFR overexpressed glioma cell line, and good cytotoxicity confirms the proposed pathway. These findings suggest that compounds **5a**, **5e** and **5n** warrant further investigation as lead molecules for the development of targeted therapies for liver, glioma and lung cancers.

Received 3rd December 2025
Accepted 6th April 2026

DOI: 10.1039/d5ra09341d

rsc.li/rsc-advances

1 Introduction

Cancer, characterized by the abnormal growth of cells in the body, is a major global health concern. According to the American Cancer Society (ACS), it is estimated that cancer causes approximately 1700 deaths daily, contributing to around 15% of all human deaths worldwide. Cancer cells often evade apoptosis, leading to unchecked growth and angiogenesis—hallmarks of all cancer types.[1–4] Apoptosis is essential for preventing cancer, and targeting this process is a highly effective cancer treatment strategy. Many anticancer drugs focus on various stages of the intrinsic and extrinsic apoptotic pathways.[5,6]

Lung cancer is one of the most prevalent cancers, with the highest rates of morbidity and mortality globally. Despite existing chemotherapeutic treatments, many are inadequate due to serious side effects and drug resistance.[7] Therefore, developing safe and effective new treatments for lung cancer is critical. According to global cancer statistics from 2018, lung cancer accounts for 11.6% of all diagnosed cancer cases and is the leading cause of cancer death, responsible for 18.4% of all cancer-related deaths. Lung cancer is primarily classified into two histological groups: Small Cell Lung Cancer (SCLC) and Non-Small Cell Lung Cancer (NSCLC), with NSCLC accounting for approximately 85% of lung cancers. NSCLC is further divided into adenocarcinoma, squamous cell carcinoma, and large cell carcinoma.

A significant challenge in treating NSCLC is that when one of the targeted pathways in signal transduction is blocked, others can serve as escape mechanisms for cancer cells.[8–11]

Thienopyran is a prominent heterocyclic structure that serves as the foundation for many pharmacologically significant compounds, particularly those with anticancer properties.[11] Fused pyran[12–19] derivatives have shown promising results in cancer treatment by targeting cellular pathways that inhibit cancer cell growth, induce apoptosis, and disrupt vital

[a]*Department of Neurological Surgery, University of Pittsburgh, 15213, USA*
[b]*Department of Chemistry, Sri Venkateshwara College, Delhi, 110021, India*
[c]*Dr B. R. Ambedkar Center for Biomedical Research, University of Delhi, North Campus, Delhi, 110007, India*
[d]*Department of Chemistry, Faculty of Science, Umm Al-Qura University, Makkah, 21955, Saudi Arabia*
[e]*Department of Chemistry, University of Delhi, North Campus, Delhi, 110007, India. E-mail: rpratap@chemistry.du.ac.in; ramendrapratap@gmail.com*
[f]*Department of Biologics, College of Pharmacy, Gachon University, Hambakmoeiro 191, Yeonsu-gu, Incheon 21924, Republic of Korea*

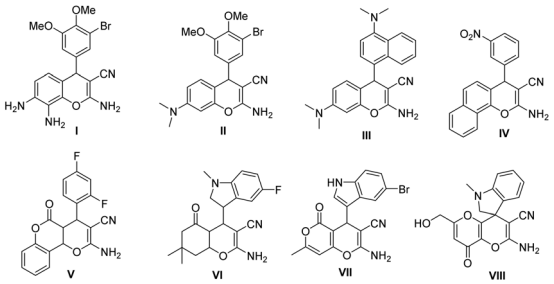

Fig. 1 Structures of potential pyran-based anticancer agents.

processes necessary for tumour progression. These compounds also exhibit a range of pharmacological activities, including antimicrobial, antitubercular, antioxidant, analgesic, anti-leishmanial, antiplatelet, FPR1 antagonist, and anticonvulsant properties.[20–26] Among these, the chromene analogues EPC2407 (Crolibulin, I) stand out as a promising agent for disrupting blood vessels in tumours and inducing apoptosis in advanced solid tumours. It has shown effectiveness in phase I clinical trials for patients with advanced thoracic and abdominal tumours and is currently in phase I/II trials in combination with cisplatin for anaplastic thyroid cancer (ATC). Similarly, MX58151 (II) has been identified as a caspase activator and tubulin inhibitor, while SP-6-27 (III) demonstrates high potency against glioma, melanoma, and prostate cancer cell lines due to its antiproliferative activity.[18,19] Other chromene analogues, such as LY290181 (IV), fluorine-containing pyrano-chromenes (V) and (VI), and indole-substituted tetrahydro-chromene (VII) [Fig. 1], have also been reported as potent anticancer agents.[27,28] Despite progress in developing chemotherapeutic agents, the development of new, target-specific anticancer drugs with minimal side effects to address drug resistance is always required.[29–31] Various thiophene-fused heterocycles are explored for anticancer activity and show very good activity[32] using different targets[39] (Table 1). The thieno[3,2-*c*]pyran nucleus is well explored for its photophysical properties, role as a metal sensor, such turn on sensor for Zn^{2+}.[11*d*] Additionally, this class of compounds are also studied for their synergistic antibacterial properties.[11*e*] The anticancer properties of this compound were not explored, so we decided to explore the anticancer activity, as it contains both thiophene and pyran rings fused in the same nucleus.

The structural flexibility of fused pyran derivatives allows the synthesis of compounds with customised properties, optimising their anticancer efficacy and minimising off-target effects.[32,33]

By introducing diverse functional groups and modifying specific regions of the fused pyran scaffold, researchers have improved potency and pharmacokinetics, resulting in better bioavailability and target specificity. Consequently, a series of functionalized thieno[3,2-*c*]pyran derivatives has been synthesized to evaluate their anticancer efficacy against various cancer cell lines, study their mechanisms of action, and conduct *in silico* ADMET predictions to assess their drug-likeness properties.[18,19]

2 Result and discussion

2.1 Chemistry

2.1.1 Synthesis of various functionalized thieno[3,2-*c*] pyran. To evaluate the anticancer activity, we designed various multifunctional 6-aryl/5,6-diaryl-thieno[3,2-*c*]pyrans and 11-oxo-5,11-dihydro-4*H*-benzo[*h*]thieno[3,2-*c*]chromenes and their synthesis was carried out by using the reported methodology.[33] To obtain the desired compounds, various functionalized isolated and fused 2*H*-pyran-2-ones **3** were used as precursors. The reaction of methyl 2-cyano-3,3-dimethylthioacrylate **1** and different aryl methyl ketones, deoxy-benzoin/anisoin, and 1-tetralone in DMSO using potassium hydroxide as a base.[34,35]

We used the precursor and synthesized the thieno[3,2-*c*] pyran[36,37] using triethylamine as a base under a green approach. We synthesized various 6-aryl/5,6-diaryl-thieno[3,2-*c*]pyrans **5a–l**, 6-aryl-5-methyl-thieno[3,2-*c*]pyrans **5m** and methyl 1-amino-11-oxo-5,11-dihydro-4*H*-benzo[*h*]thieno[3,2-*c*]chromene-2-carboxylates **5n** and **5o** by treatment of synthesized precursor with methyl thioglycolate. All reactions were carried out in water using CTAB as surfactant and Et_3N as a base at 85 °C. The reaction was heated at the given temperature for 2–4 hours, depending on the derivatives. After completion of the reaction, the obtained precipitate was filtered and washed with water. The compounds were dried and recrystallized from ethanol and further tested.

Considering the structure-activity relationship (SAR), we synthesized a series of thienopyran derivatives with various substitutions on the thiophene and pyran rings. We have incorporated different groups such as $-NO_2$, alkyl, alkoxy, esters, amines and halides to study their outcome on activity.

Additionally, this study represents the first exploration of these compounds as potential anti-cancer agents. We introduced substitutions at the 6th position of the pyran ring with an aromatic group and at the 4th and 5th positions of the thiophene ring with $-NH_2$ and –COOMe, respectively (Fig. 2). It was found that $-NH_2$ and –COOMe substitutions provided basic

Table 1 Biological activity of some of the thieno-fused molecules

No.	Thieno-fused molecule[39]	Biological target and/or activity
1	Thieno[3,2-*d*]pyrimidine	CDK inhibition; apoptosis induction
2	Thieno[2,3-*d*]pyrimidine	EGFR and DHFR inhibition and anticancer cytotoxicity
3	Thieno[2,3-*d*][1,2,4]triazolo-pyrimidine hybrids	Anticancer activity *via* kinase inhibition
4	Oxadiazole-incorporated thieno heterocycles	Cytotoxic activity against A549 lung cancer cells
5	Thieno[3,2-*e*]pyrrolo[1,2-*a*]pyrimidine	Antitumor activity in pulmonary metastatic models
6	Thieno[3,2-*c*]pyran	Antibacterial activity, anticancer (this work)

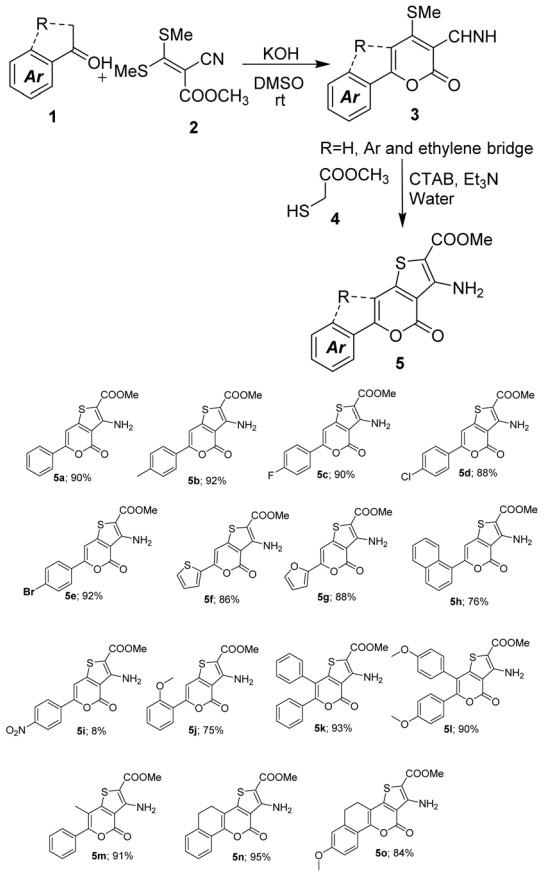

Fig. 2 Synthesis of different thieno[3,2-*c*]pyran-2-ones [**5a–5o**]. Reagents and conditions: all the reactions were performed by stirring 1 (1.0 mmol), 2 (1.5 mmol) and *CTAB* (0.25 mmol) + Et_3N (30 mol%) in 15 mL of water at 85 °C.

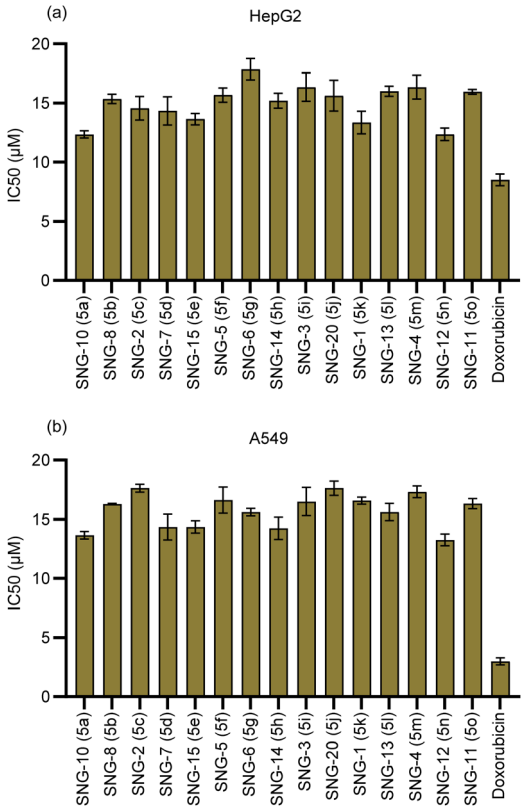

Fig. 3 (a) Cytotoxic effects of synthesized compounds (**5a–o**) on HepG2; (b) cytotoxic effects of synthesized compounds (**5a–o**) on A549 cells.

binding sites that enhanced biological activity. Modifications to the pyran ring revealed that compounds with an aromatic group alone at the 6th position demonstrated effective IC_{50} values, as illustrated by **5a** and **5n**.

2.2 Biological study

2.2.1 Cytotoxic activity of synthesized compounds. All synthesized compounds (**5a–o**) were evaluated for their cytotoxic potential against two human cancer cell lines, hepatocellular carcinoma (HepG2) and lung carcinoma (A549), using the cell viability assay. Among the series, compounds **5a** and **5n** exhibited the most potent cytotoxic effects. The IC_{50} values for **5a** were 13.65 ± 0.32 μM in HepG2 cells and 12.35 ± 0.30 μM in A549 cells, while **5n** displayed IC_{50} values of 13.26 ± 0.32 μM in HepG2 and 12.36 ± 0.30 μM in A549 cells (Fig. 3a and b). These values were the lowest among all tested compounds, indicating that **5a** and **5n** have superior antiproliferative activity in both cell lines.

Cell viability was assessed after 48 h of treatment with the indicated compounds at varying concentrations. The percentage of viable cells was calculated relative to untreated controls. IC_{50} values (concentration causing 50% inhibition of cell viability) were determined. Data represent mean ± SD of three independent experiments performed in triplicate. Compounds **5a** and **5n** exhibited the highest cytotoxicity, with the lowest IC_{50} values in both (a) HepG2 and (b) A549 cells.

2.2.2 Effect of compounds on cell cycle progression. To further explore the mechanism of cytotoxicity, we assessed the impact of **5a** and **5n** on cell cycle progression in HepG2 cells using propidium iodide (PI) staining and flow cytometry. Treatment with both compounds resulted in significant G1 phase arrest compared to untreated controls, suggesting that the observed growth inhibition may be associated with the interruption of cell cycle progression (Fig. 4a). These data indicate that **5a** and **5n** can interfere with the normal cell cycle, thereby reducing cellular proliferation.

2.2.3 Induction of apoptosis by 5a and 5n. The apoptotic potential of **5a** and **5n** was evaluated at their respective IC_{50} concentrations in HepG2 cells using Annexin V-FITC/PI staining. Flow cytometric analysis demonstrated that compound **5a** induced apoptosis in approximately 12–14% of cells, whereas **5n** triggered apoptosis in only 6–7% of cells (Fig. 4b). These results suggest that, although both compounds can arrest the cell cycle at G1, **5a** is more effective at promoting apoptotic cell death compared to **5n** under the tested conditions (Fig. 4b).

In summary, compounds **5a** and **5n** exhibited the strongest cytotoxic effects among the synthesized compounds with low micromolar IC_{50} values in both HepG2 and A549 cells. Cytotoxicity is likely mediated by G1 phase cell cycle arrest, with

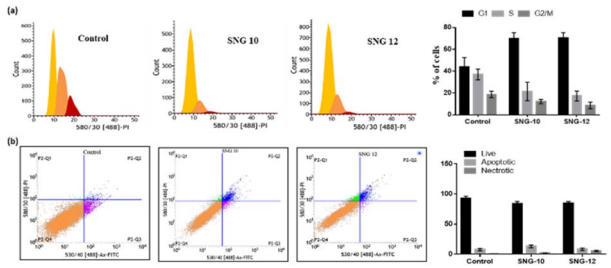

Fig. 4 Effects of compounds **5a** (SNG 10) and **5n** (SNG 12) on cell cycle progression and apoptosis in A549 cells. (a) Cell cycle distribution was analysed by flow cytometry using propidium iodide (PI) staining after 48 h treatment with SNG-10 (**5a**) or SNG-12 (**5n**). Both compounds induced significant G1 phase arrest compared to untreated controls. (b) Apoptotic activity was measured using Annexin V-FITC/PI staining following 48 h exposure to **5a** or **5n**. Compound **5a** induced higher apoptosis (~12–14%) compared to **5n** (~6–7%). All values are presented as mean ± SD of three independent experiments.

apoptosis contributing partially to the antiproliferative effect, particularly for compound **5a**. These findings identify **5a** as a promising lead for further mechanistic and therapeutic studies.

2.2.4 Effect of selected compounds on cell viability in EGFR-expressing LN229 glioblastoma cells. To evaluate the cytotoxic potential of the compounds **5a**, **5d**, **5e** and **5n** against an EGFR-expressing glioblastoma cell line, the MTT cell viability assay was performed in LN229 cells at a fixed concentration of 26 μM. Both freshly dissolved (in media) and pre-incubated (dissolved in PBS at 25 °C for 24 hours) formulations of each compound were tested to assess the influence of solubilization conditions on biological activity. DMSO was used as the vehicle control, and all results were normalised to DMSO-treated cells (100% viability) (Fig. 5).

Quantification of cell viability expressed as a percentage of DMSO control is presented in Figure B. Treatment with all compounds at 26 μM resulted in a significant reduction in cell viability, with values ranging from approximately 40% to 60% relative to the vehicle control. Statistical analysis confirmed that all compound-treated groups showed highly significant reductions in cell viability compared to DMSO (***$p < 0.001$), indicating potent cytotoxic activity against LN229 cells at this concentration.

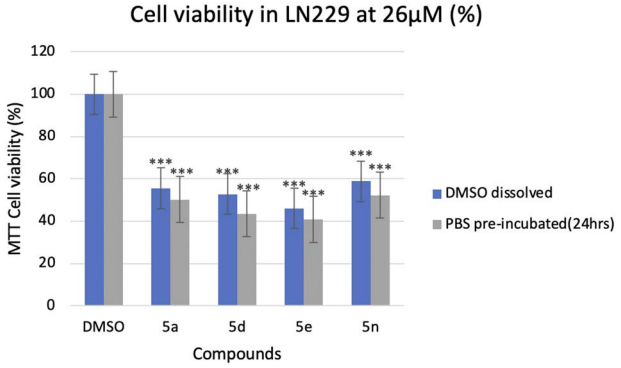

Fig. 5 MTT %age cell viability assay of selected compounds in LN229 at 26 μM concentration for 48 h of treatment (p-value <0.05(*), <0.01(**), <0.001(***)are considered significant; graph plotted ± SEM).

Among the PBS dissolved compounds, **5d** and **5e** (PBS pre-incubated formulations) demonstrated the most pronounced cytotoxicity, reducing cell viability to approximately 40–43%, suggesting near-maximal growth inhibition at 26 μM. In contrast, compounds **5a** and **5n** show relatively moderate cytotoxicity, with viability values in the range of 55–60%, though still significantly different from the control.

2.2.5 Stability of compound 5a in LN229 glioma cells. The stability of compound **5a** was evaluated in the LN229 glioblastoma cell line, with endogenously amplified EGFR, using the MTT cell viability assay at a concentration of 13 μM. Treatment of LN229 cells with compound **5a** resulted in approximately 55% cytotoxicity, indicating antiproliferative activity at the tested concentration. This reduction in cell viability was statistically significant ($p < 0.001$), as determined by comparison with the DMSO control group. To assess the stability and functional integrity of compound **5a** under physiologically relevant pre-incubation conditions, the compound was pre-incubated in PBS at 26 °C for 48 and 72 hours before treatment. Both PBS-pre-incubated formulations (PBS-48 and PBS-72) retained substantial cytotoxic activity, with cell viability values remaining statistically significantly reduced compared to the DMSO control ($p < 0.001$). However, a reduction of approximately 5–10% in cytotoxic potency was observed relative to freshly prepared compound **5a**, which is also possible due to media compound interaction (Fig. 6).

A similar trend was observed when compound **5a** was pre-incubated in fetal calf serum (FCS)-containing media under identical conditions (FCS-48 and FCS-72). The FCS-pre-incubated samples likewise demonstrated statistically significant cytotoxicity compared to the DMSO control ($p < 0.001$), with a comparable 5–10% attenuation in antiproliferative activity relative to the freshly dissolved compound. Collectively, these results demonstrate that compound **5a** exerts significant cytotoxic activity against EGFR-expressing LN229 glioblastoma cells at 13 μM, and that this activity is largely preserved following pre-incubation under both aqueous and serum-containing conditions for up to 72 hours, supporting the stability and

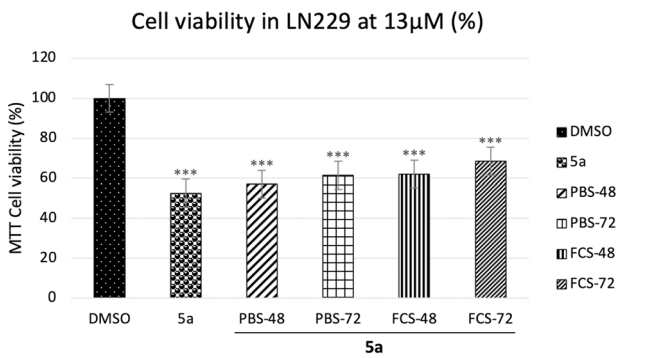

Fig. 6 MTT cell viability assay in LN229 at 13 μM concentration for 48 h of treatment to study the stability of compounds in; DMSO, compound preincubated in PBS and FCS for 48 h and 72 h before treatment (p-value <0.05(*), <0.01(**), <0.001(***)are considered significant; graph plotted ± SEM).

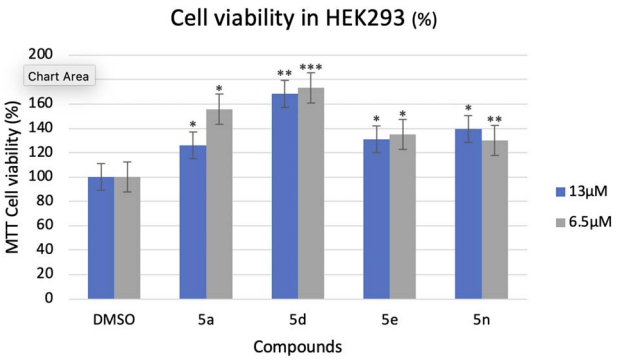

Fig. 7 MTT cell viability assay in HEK293 treatment with compounds (**5a**, **5d**, **5e** and **5n**) at 13 μM and 6.5 μM concentration for 48 h treatment (*p*-value <0.05(*), <0.01(**), <0.001(***) are considered significant; graph plotted ± SEM).

translational potential of the compound under physiological conditions.

The stability of compounds was also confirmed by mass spectrometry. We have recoded the chromatogram of compound **5a** after treatment with PBS for 48 and 72 h at 26 °C. Each chromatogram shows no decomposition of compounds and suggests their stability during testing against the cell line (see SI; Fig. S2–S4).

2.2.6 *In vitro* cytotoxicity of compounds in HEK293 cells. To evaluate the biocompatibility of the synthesized compounds, an MTT cell viability assay was performed on HEK293 cells following 48 hours of treatment at two concentrations, 13 μM and 6.5 μM. None of the tested compounds (**5a**, **5d**, **5e**, and **5n**) exhibited cytotoxic effects on the HEK293 cell line at the tested concentrations. Instead, all treatment groups showed an increase in absorbance values compared to the DMSO control (Figure C). Compounds **5a**, **5e**, and **5n** showed statistically significant increases in metabolic activity/cell viability compared to the control ($p < 0.05$ or $p < 0.01$) (Figure D). There were no drastic differences in cell response between the 13 μM and 6.5 μM doses across the tested compounds, suggesting a plateau in the proliferative or metabolic response within this concentration range (Fig. 7 and 8).

Overall, the data indicate that compounds **5a**, **5d**, **5e**, and **5n** are non-toxic to HEK293 cells under the specified conditions and may promote cell proliferation or increased metabolic activity.

2.2.7 Molecular docking analysis. Molecular docking simulations were carried out using Maestro to evaluate the binding affinities and interaction profiles of reference and test compounds-specifically, compounds **5a** and **5n** against key oncogenic targets: Epidermal Growth Factor Receptor (EGFR) for lung cancer and Vascular Endothelial Growth Factor Receptor 2 (VEGFR-2) for liver cancer. These simulations aimed to correlate the *in-silico* binding behaviours with biological assay data and to provide insight into the structural determinants governing receptor–ligand interactions. The crystallographic structure of EGFR in complex with erlotinib (PDB ID: 4HJO) served as a reference for binding site validation. To confirm docking reliability, erlotinib was redocked into the EGFR active site, demonstrating accurate pose reproduction. A comprehensive screening of the series of compounds was conducted, and high-scoring candidates were shortlisted. Among them, compounds **5a** and **5n** exhibited superior docking scores and were selected for further investigation.

Compound **5a** exhibited favourable binding to EGFR, with a docking score of −7.925. A hydrogen bond (3.25 Å) was observed with Cys773, a polar residue. The binding pocket consisted of hydrophobic residues (Ala719, Leu764, Leu820, Leu834, and Val702), basic residues (Lys721, Gly772), acidic residues (Asp86), and polar uncharged residues (Thr766). These interactions indicate a stable and specific binding conformation, illustrated in Fig. 9(a) and (b).

Similarly, compound **5n** demonstrated a high docking score of −7.871 with EGFR. It formed a hydrogen bond (2.0 Å) *via* a bridging water molecule, enhancing binding specificity. The residues surrounding the binding site included Asp831 (acidic), Thr830 (polar), Lys721, Gly772 (basic), Val702, Leu794, Leu768, Leu820 (hydrophobic), and Met769 (nonpolar). This configuration supports a robust interaction profile, detailed in Fig. 10(c) and (d).

Compound **5a** displayed a strong binding affinity toward VEGFR-2, yielding a Glide docking score of −8.834. It formed

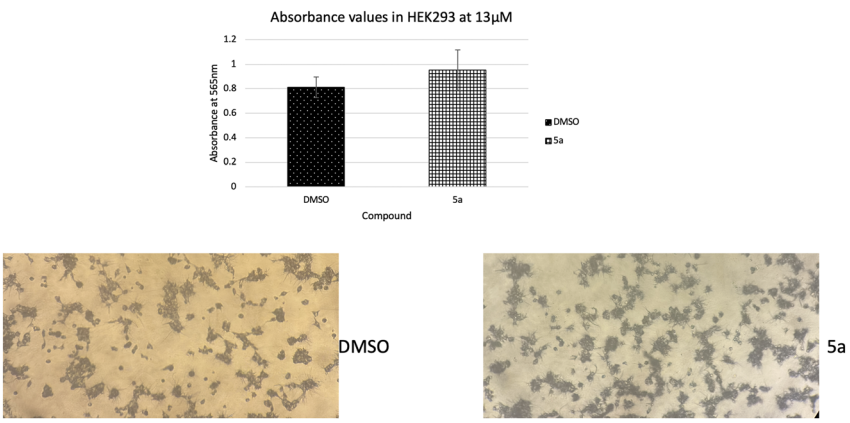

Fig. 8 HEK293 Cell images taken after incubation with MTT reagent at 565 nm, cell number is the same, but the intensity of crystal formation is higher in cells treated with **5a**.

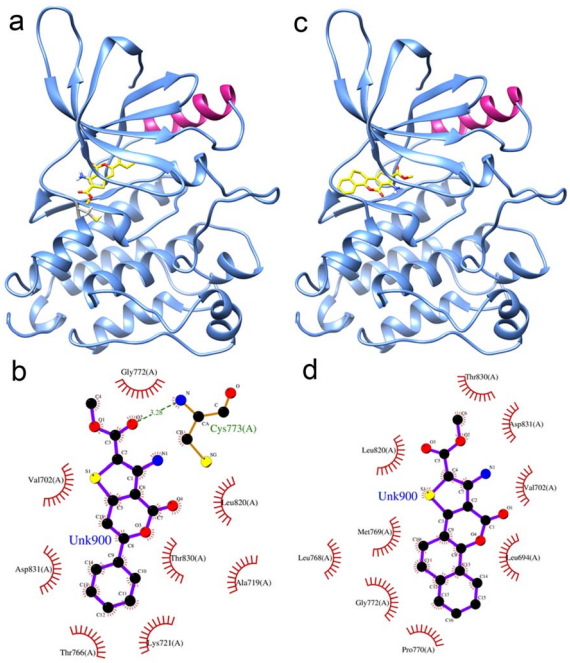

Fig. 9 Illustrative depiction of the ligand–protein complexes. The most favourable binding conformations of compounds **5a** and **5n** with EGFR are shown, exhibiting high docking scores of (a) −7.925 kcal mol^{-1} and (b) −7.871 kcal mol^{-1}, respectively. The interaction profiles of **5a** (c) and **5n** (d) are visualized through 2D molecular interaction diagrams generated using LigPlot+ v.2.2.4. In these diagrams, green dashed lines indicate hydrogen bonds along with their bond distances, while red spiked arcs highlight the residues participating in hydrophobic.

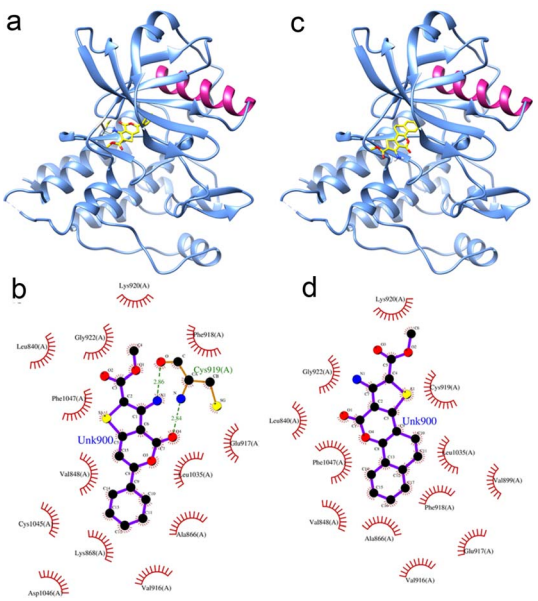

Fig. 10 Illustrative depiction of the ligand–protein complexes. The most favourable binding conformations of compounds **5a** and **5n** with VEGFR-2 are shown, exhibiting high docking scores of (a) −8.834 kcal mol^{-1} and (b) −8.994 kcal mol^{-1}, respectively. The interaction profiles of **5a** (c) and **5n** (d) are visualized through 2D molecular interaction diagrams generated using LigPlot+ v.2.2.4. In these diagrams, green dashed lines indicate hydrogen bonds along with their bond distances, while red spiked arcs highlight the residues participating in hydrophobic.

a key hydrogen bond (2.84 Å) with the thiol group of Cys919, a polar uncharged residue. The residues within 3 Å of the ligand included a combination of aromatic (Phe918), hydrophobic (Val916, Val899, Val848, Ala866, Leu840, Leu1035), basic (Lys920, Lys868, Gly922), acidic (Glu917, Asp1046), and polar amide residues (Cys1045). This network of hydrophobic and polar interactions contributed to the stable binding conformation observed in Fig. 10 (a) and (b).

In comparison, compound **5n** showed an even higher affinity with a docking score of −8.994. A notable π–π stacking interaction (2.7 Å) was observed with Phe918, further stabilizing the complex. The surrounding pocket was similarly composed of hydrophobic (Val916, Val899, Val848, Ala866, Leu840, Leu1035), basic (Lys920, Gly922), acidic (Glu917), and polar (Cys919) residues, facilitating strong hydrophobic interactions and potential functional activity, as depicted in Fig. 10(c) and (d).

As reported, compounds **5a** and **5n** exhibited the most potent antiproliferative effects among the tested series, with very similar IC_{50} values in both HepG2 and A549 cell lines. In HepG2 cells, compound **5a** showed an IC_{50} of 13.65 ± 0.32 μM, while **5n** exhibited an IC_{50} of 13.26 ± 0.32 μM. Likewise, in A549 cells, the IC_{50} values were 12.35 ± 0.30 μM for **5a** and 12.36 ± 0.30 μM for **5n**. These differences are minimal and fall within experimental variability, indicating that both compounds possess comparable cytotoxic potency at the cellular level.

Although compound **5n** demonstrated a slightly better VEGFR-2 docking score, cytotoxic activity reflects an integrated cellular response rather than binding affinity alone. The comparable IC_{50} values suggest that both compounds achieve similar levels of growth inhibition, while differences in apoptotic induction may arise from factors beyond receptor binding, such as intracellular uptake, metabolic stability, or differential engagement of downstream signalling pathways. Importantly, compound **5a** showed consistent and robust cytotoxicity across both cell lines, which may explain its relatively stronger apoptotic response despite a marginally lower docking score.

The standard drug Doxorubicin, used as a control, displayed comparatively lower binding affinities with VEGFR-2 and EGFR, scoring −7.157 and −5.252, respectively. These results underscore the enhanced binding potential of the novel compounds **5a** and **5n** over the reference compound, reinforcing their candidacy for further biological evaluation.

3 Experimental section

3.1 Materials

Commercially available reagents and solvents from TCI Chemicals, Sigma Aldrich, and Alfa Aesar were used without further purification. Reactions were monitored by analytical thin-layer chromatography (TLC) and were conducted in dry glassware. Infrared (IR) spectra were recorded using a PerkinElmer AX-1 spectrophotometer, with stretching frequencies reported as

wave numbers (cm^{-1}). ^1H and ^{13}C NMR spectra were acquired on 400 MHz and 100 MHz NMR spectrometers, respectively. $CDCl_3$ (from Eurisotop) was used as the solvent to obtain the NMR data and chemical shifts reported in parts per million (ppm) relative to $CDCl_3$, where δ 7.26 ppm and δ 77.00 ppm served as internal standards for ^1H and ^{13}C NMR, respectively. Additionally, DMSO-d_6 (from Eurisotop) was used as a solvent, with chemical shifts referenced in ppm relative to DMSO-d_6, where δ 2.50 ppm and δ 39.52 ppm were used as internal standards for ^1H and ^{13}C NMR, respectively. NMR signal patterns are designated as s (singlet), d (doublet), dd (doublet of doublets), t (triplet), m (multiplet), and bs (broad singlet). Extraction and chromatography were performed with reagent-grade solvents, and yields are reported for chromatographically pure materials.

3.2 Synthesis of compounds

3.2.1 General protocol for synthesis of methyl 3-amino-4-oxo-6-aryl-*4H*-thieno[3,2-*c*]pyran-2-carboxylate. A mixture of 4-(methylthio)-2-oxo-6-aryl-2*H*-pyran-3-carbonitriles (1.0 mmol), methyl thioglycolate (1.5 mmol) was dissolved in distilled water (15 mL) followed by the addition of CTAB (0.25 mmol). Then triethylamine (30 mol%) was added, and the mixture was stirred for 2–3 h at 85 °C. After completion of the reaction, the mixture was cooled down to room temperature. The obtained precipitate was filtered and washed with hot distilled water. Finally, the product was dried and recrystallized from hot ethanol. The characterization data for the synthesized compounds are reported earlier.[33b]

3.3 Cell line study

3.3.1 IC_{50} and cell viability assay. A549, HepG2, LN229 and HEK293 cells were procured from the National Centre for Cell Science (NCCS), Pune, India. A549, HepG2, LN229 and HEK293 cells were maintained in DMEM (Gibco) supplemented with 10% fetal bovine serum and 1% penicillin–streptomycin at 37 °C in a humidified incubator with 5% CO_2. Cells were lyophilized, counted with a Countess cell counter (Invitrogen), and seeded in clear-bottom 96-well plates at densities optimized to remain in logarithmic growth over the assay period (A549: 5000 cells/well; HepG2: 8000 cells/well in 100 μL complete medium). After allowing cells to attach for 16–18 h, the medium was replaced with 100 μL fresh medium containing compounds. Each concentration was tested in technical triplicate, and experiments were repeated at least three times. After compound exposure for the indicated time (24, 48, or 72 h, depending on the experiment), cell viability was measured using the PrestoBlue™ Cell Viability Reagent (Thermo Fisher) according to the manufacturer's instructions. Briefly, plates were equilibrated to room temperature for 10 min, then 10 μL PrestoBlue reagent (10% v/v final) was added directly to each well (final volume 110 μL). Plates were protected from light and incubated at 37 °C for 10–30 min (incubation time optimized per cell line to ensure signal remained within the linear range). Fluorescence was measured on a plate reader using excitation at 560 nm and emission at 590 nm. For each plate, blank wells containing medium + PrestoBlue (no cells) and vehicle control wells (cells + vehicle) were included. Raw fluorescence values were background-subtracted (blank) and normalized to vehicle control wells. Percentage viability was calculated as:

$$\%\ \text{viability} = \frac{\text{RFU treated} - \text{RFU blank}}{\text{RFU vehicle} - \text{RFU blank}} \times 100$$

Dose–response curves and half-maximal cytotoxic concentration (IC_{50}) values were determined by nonlinear regression (log [inhibitor] *vs.* response − variable slope) using GraphPad Prism. Data are presented as ± SEM from three independent experiments.

3.4 Cell cycle and apoptosis assays

3.4.1 Cell cycle assay. Cell cycle distribution was determined using the propidium iodide (PI) uptake method, following previously described protocols.[38] Briefly, cells treated with the indicated compounds (*e.g.*, SNG-10 (**5a**) and SNG-12 (**5n**)) were harvested, washed three times with phosphate-buffered saline (PBS), and fixed in 70% ethanol at −20 °C for 30 minutes. Fixed cells were then centrifuged, washed three times with PBS, and resuspended in a staining buffer containing RNase A (10 μg mL^{-1}) and propidium iodide (1 μg mL^{-1}). The mixture was incubated in the dark at room temperature for 30 minutes, allowing PI to intercalate with DNA. Cell cycle phases (G0/G1, S, G2/M) were analysed using a BD FACS Influx flow cytometer, and data were processed using FlowJo software. Experiments were performed in triplicate, and the percentage of cells in each phase was calculated relative to untreated controls.

3.4.2 Apoptosis assay. Apoptotic cell death was assessed using FITC-labelled annexin V and propidium iodide (PI) staining, as previously described.[39] Cells treated with the active compounds (**5a** or **5n**) were detached using trypsin, washed twice with PBS, and resuspended in 100 μL of annexin V binding buffer. Annexin V-FITC (5 μL) was added to the cell suspension, and cells were incubated in the dark at room temperature for 15 minutes. Subsequently, propidium iodide (5 μL) was added immediately before analysis. Apoptotic cells were quantified using a BD FACS Influx flow cytometer, distinguishing early apoptotic (annexin V^+/PI^-), late apoptotic/necrotic (annexin V^+/PI^+), and viable cells (annexin V^-/PI^-). All experiments were performed in triplicate, and data are presented as mean ± SD.

3.5 MTT cell viability assay against LN229 and HEK293 cell lines[40]

Cell viability was assessed using the 3-(4,5-dimethylthiazol-2-yl)-2,5-diphenyltetrazolium bromide (MTT) colorimetric assay. LN229 and HEK293 cells were harvested and seeded in 96-well flat-bottom tissue culture plates at a density of 5×10^3 cells per well in a final volume of 100 μL complete DMEM per well. Cells were allowed to adhere and equilibrate overnight at 37 °C with 5% CO_2 before treatment. Following overnight incubation, the culture medium was replaced with 100 μL of fresh serum-free DMEM containing dilutions of the compounds at concentrations 26 μM, 13 μM, 6.5 μM. Test compounds were prepared as stock solutions in dimethyl sulfoxide (DMSO) and further

diluted in DMEM. After 48 hours, the medium was carefully aspirated from each well without disturbing the cell monolayer. Subsequently, 10 μL of the MTT stock solution (5 mg mL^{-1}) was added to each well along with 90 μL of serum-free DMEM, to a final MTT concentration of 1 mg mL^{-1} per well. Plates were incubated at 37 °C for 4 hours in dark. The insoluble purple formazan crystals formed in each well were dissolved by adding 200 μL of DMSO to each well. Plates were placed 37 °C for 20 minutes. The absorbance was measured at 565 nm in ELISA plate reader (TECAN).

3.6 Molecular docking

The chemical structures of the lead compounds, **5a** and **5n**, were initially constructed in ChemDraw (.cdx format) and subsequently converted to the Maestro-compatible .maegz format using Maestro version 11.8 (Schrödinger, LLC). Molecular docking studies were conducted using the Glide module. High-resolution crystal structures relevant to lung (PDB ID: 4HJO)[40,41] and liver cancer (PDB ID: 4ASD)[42] were retrieved from the Protein Data Bank. These protein models were pre-processed using the Protein Preparation Wizard in Maestro, which included hydrogen addition, assignment of appropriate protonation states, removal of water molecules, and energy minimization utilizing the OPLS-2005 force field. Ligand preparation was carried out using the LigPrep tool, with Epik used to generate ionization states at a physiological pH of 7.0, applying the same OPLS-2005 force field. Docking simulations were executed using Glide in Extra Precision (XP) mode to ensure accurate binding predictions. The resulting docked complexes were visualized and analysed with PyMOL version 2.5.[43]

4 Conclusions

In this study, we synthesized a series of compounds (**5a–o**) and evaluated their cytotoxic potential against human hepatocellular carcinoma (HepG2) and lung carcinoma (A549) cell lines. Among all tested compounds, **5a** and **5n** exhibited the best antiproliferative activity, with IC_{50} values in the low micromolar range. The comparable activity in both HepG2 and A549 cells suggests that these compounds possess broad cytotoxic effects against distinct cancer types, highlighting their potential as lead molecules for further anticancer development. Additionally, compound **5e** also exhibits good activity against Glioma cancer with an IC_{50} of 26 μM. Further study of these compounds is going on.

The mechanism underlying the observed cytotoxicity was explored through cell cycle analysis. Both **5a** and **5n** induced significant G1 phase arrest in HepG2 cells, indicating that these compounds interfere with the normal progression of the cell cycle. G1 arrest is often associated with inhibition of DNA synthesis and the activation of cellular checkpoints, which can slow proliferation and sensitize cells to apoptotic signals. Our findings suggest that disruption of cell cycle machinery is a key contributor to the growth-inhibitory effects of these compounds.

Further investigation into apoptosis induction revealed a differential effect between the two compounds. While **5a** induced apoptosis in approximately 12–14% of cells, **5n** showed a relatively modest apoptotic effect (6–7%). These results indicate that, although both compounds can arrest the cell cycle, compound **5a** more effectively triggers programmed cell death, which may explain its slightly superior antiproliferative activity. The partial contribution of apoptosis to overall cytotoxicity suggests that G1 arrest and apoptosis act in concert to inhibit cell growth, with cell cycle arrest likely being the primary mechanism.

Further, the testing of selected compounds against the normal cell line HEK293 under the same conditions and concentration shows no cytotoxicity. We also confirmed the role of EGFR inhibition in the proposed study. The selected compounds were tested against the EGFR-expressing glioma cell line, and good cytotoxicity confirms that the proposed pathway is probable.

In conclusion, this study demonstrates that compounds **5a** and **5n** are effective cytotoxic agents, with compound **5a** showing the most promising activity. The ability of these compounds to inhibit proliferation through cell cycle arrest and apoptosis provides a strong basis for further optimization and development as potential anticancer therapeutics.

Author contributions

A.J. was involved in an apoptotic study and D.K.Y. was involved in a molecular docking study. R.P. was involved in designing the concept, the synthetic protocols and writing the manuscript. Pooja and IA were involved in the synthesis and writing of the manuscript. L.T. and A.K.Y. was involved in further study of compounds on normal and glioma cell lines and further biological study. They are also involved in manuscript preparation.

Conflicts of interest

There are no conflicts to declare.

Data availability

The data supporting this article have been included as part of the supplementary information (SI). Data for these compounds are reported in *Biomedicine & Pharmacotherapy*, 2021, **142**, 112084. *RSC Advances* 2016, 6, 85515–85520. *RSC Adv.*, 2025, **15**, 12117–12124. Supplementary information: ^{1}H and ^{13}C spectral data and spectra of compound **5a–o**, LN229 cell images taken after incubation with MTT, dose response curves and IC_{50} plots for all the synthesized compounds. See DOI: https://doi.org/10.1039/d5ra09341d.

Acknowledgements

Pooja thanks ANRF for providing the research funding (EEQ/2023/000121) and Sri Venkateswara College, University of Delhi, for providing research lab space and facility. RP thanks CSIR, New Delhi, for research funding *via* project number 02/0469/23/EMR II. RP thanks AvH Foundation, Germany, for providing funding under the alumni visit program. RP thanks IOE for providing research funding during 2025–26.

Notes and references

1 R. L. Siegel, K. D. Miller and A. Jemal, *Ca-Cancer J. Clin.*, 2019, **69**, 7.
2 R. L. Siegel, K. D. Miller and A. Jemal, *Ca-Cancer J. Clin.*, 2016, **66**, 7.
3 H. Sung, J. Ferlay, R. L. Siegel, M. Laversanne, I. Soerjomataram, A. Jemal and F. Bray, *Ca-Cancer J. Clin.*, 2021, **71**, 209.
4 A. Bistrović Popov, R. Vianelo, P. Grbčić, M. Sedić, S. K. Pavelić, K. Pavelić and S. Raić-Malić, *Molecules*, 2021, **26**, 3334.
5 C. Pfeffer and A. Singh, *Int. J. Mol. Sci.*, 2018, **19**, 448.
6 A. Kamal, A. Mallareddy and P. Suresh, *Heterocyclics as Inducers of Apoptosis*, Springer, 2012, p. 45.
7 H. Zhou, S. Wu, S. Zhai, A. Liu, Y. Sun, R. Li, Y. Zhang, S. Ekins, P. W. Swaan, O. B. Fang, B. Zhang and B. Yan, *J. Med. Chem.*, 2008, **51**, 1242.
8 W. G. Kaelin, *Nat. Rev. Cancer*, 2005, **5**, 689.
9 A. T. Fojo, K. Ueda, D. J. Slamon, D. G. Poplack, M. M. Gottesman and I. Pastan, *Proc. Natl. Acad. Sci. U. S. A.*, 1987, **84**, 265.
10 M. M. Gottesman, T. Fojo and S. E. Bates, *Nat. Rev. Cancer*, 2002, **2**, 48.
11 (*a*) N. Kartner, J. R. Riordan and V. Ling, *Science*, 1983, **221**, 1285; (*b*) S. N. Sahu, M. K. Gupta, T. Jadhav, P. Yadav, S. Singh, R. Misra and R. Pratap, *RSC Adv.*, 2014, **4**, 56779–56783; (*c*) S. N. Sahu, S. Singh, R. Shaw, V. J. Ram and R. Pratap, *RSC Adv.*, 2016, **6**, 85515–85520; (*d*) D. Singhal, I. Althagafi, A. Kumar, S. Yadav, A. K. Prasad and R. Pratap, *New J. Chem.*, 2020, **44**, 12019–12026; (*e*) G. R. Dwivedi, R. Rai, R. Pratap, K. Singh, S. Pati, S. N. Sahu, R. Kant, M. P. Darokar and D. K. Yadav, *Biomed. Pharmacother.*, 2021, **142**, 112084.
12 K. Fabitha, A. Kallingal, N. Maciejewska, C. G. Arya, M. Chandrakanth, N. M. Thomas, Y. Li, R. Gondru, M. Munikumar and J. Banothu, *New J. Chem.*, 2024, **48**, 8038.
13 F. M. Dean, *Naturally Occurring Oxygen Ring Compounds*, Butterworth-Heinemann, 1963, p. 176.
14 S. A. Patil, R. Patil, L. M. Pfeffer and D. D. Miller, *Future Med. Chem.*, 2013, **5**, 1647.
15 V. Raj and J. Lee, *Front. Chem.*, 2020, **8**, 1.
16 M. K. Katiyar, G. K. Dhakad, Shivani, S. Arora, S. Bhagat, T. Arora and R. Kumar, *J. Mol. Struct.*, 2022, **1263**, 133012.
17 B. Borah, K. D. Dwivedi and L. R. Chowhan, *Polycyclic Aromat. Compd.*, 2022, **42**, 5893.
18 M. S. Malik, H. Ather, S. M. Asif Ansari, A. Siddiqua, Q. M. S. Jamal, A. H. Alharbi, M. M. Al-Rooqi, R. S. Jassas, E. M. Hussein, Z. Moussa, R. J. Obaid and S. A. Ahmed, *Pharmaceuticals*, 2023, **16**, 333.
19 W. Kemnitzer, J. Drewe, S. Jiang, H. Zhang, C. Crogan-Grundy, D. Labreque, M. Bubenick, G. Attardo, R. Denis, S. Lamothe, H. Gourdeau, B. Tseng, S. Kasibhatla and X. C. Sui, *J. Med. Chem.*, 2008, **51**, 417.
20 N. R. Kamdar, D. D. Haveliwala, P. T. Mistry and S. K. Patel, *Med. Chem. Res.*, 2011, **20**, 854.
21 G. Singh, A. Sharma, H. Kaur and M. P. S. Ishar, *Chem. Biodiversity*, 2016, **87**, 213.
22 C. Bingi, E. Narender Reddy, M. Chennapuram, Y. Poornachandra, C. G. Kumar, N. Jagadeesh Babu and K. Atmakur, *Bioorg. Med. Chem. Lett.*, 2015, **25**, 1915.
23 N. D. Vala, H. H. Jardosh and M. P. Patel, *Chin. Chem. Lett.*, 2016, **27**, 168.
24 E. Rajanarendar, M. Nagi Reddy, S. Rama Krishna, K. Rama Murthy, Y. N. Reddy and M. V. Rajam, *Eur. J. Med. Chem.*, 2012, **55**, 273.
25 N. C. Lazzara, R. J. Rosano, P. P. Vagadia, M. T. Giovine, M. W. Bezpalko, N. A. Piro, W. S. Kassel, W. J. Boyko, D. L. Zubris, K. K. Schrader, D. E. Wedge, S. O. Duke and R. M. Giuliano, *J. Org. Chem.*, 2019, **84**, 666.
26 J. H. Roireau, R. J. Rosano, N. C. Lazzara, T. Chen, J. Bajsa-Hirschel, K. K. Schrader, S. O. Duke, D. Wykoff and R. M. Giuliano, *J. Agric. Food Chem.*, 2020, **68**, 9906.
27 D. Rajguru, B. S. Keshwal and S. Jain, *Med. Chem. Res.*, 2013, **22**, 5934.
28 K. Parthasarathy, C. Praveen, C. Balachandran, P. Senthil Kumar, S. Ignacimuthu and P. T. Perumal, *Bioorg. Med. Chem. Lett.*, 2013, **23**, 2708.
29 L. Braconi, E. Teodori, C. Riganti, M. Coronnello, A. Nocentini, G. Bartolucci, M. Pallecchi, M. Contino, D. Manetti, M. N. Romanelli, C. T. Supuran and S. Dei, *J. Med. Chem.*, 2022, **65**, 14655.
30 S. Wang, S. Q. Wang, Q. Teng, L. Yang, Z. Lei, X. Yuan, J. Huo, X. Chen, M. Wang, B. Yu, Z. Chen and H. Liu, *J. Med. Chem.*, 2020, **63**, 15979.
31 D. J. Hong, S. H. Jung, J. Kim, D. Jung, Y. G. Ahn, K. H. Suh and K. H. Min, *J. Enzyme Inhib. Med. Chem.*, 2020, **35**, 227.
32 M. M. Heravi and V. Zadsirjan, *RSC Adv.*, 2020, **10**, 44247.
33 (*a*) N. Kerru, L. Gummidi, S. Maddila, K. K. Gangu and S. B. Jonnalagadda, *Molecules*, 2020, **25**, 1909; (*b*) S. N. Sahu, R. Shaw, S. Yadav, I. Althagafi, M. K. Upadhyay and R. Pratap, *RSC Adv.*, 2025, **15**, 12117–12124.
34 S. Singh, I. Althagafi, P. Yadav, R. Panwar, A. Kumar and R. Pratap, *Tetrahedron*, 2014, **70**, 8879.
35 V. J. Ram, M. Nath, P. Srivastava, S. Sarkhel and P. R. Maulik, *J. Chem. Soc., Perkin Trans. 1*, 2000, 3719.
36 S. N. Sahu, M. K. Gupta, T. Jadhav, P. Yadav, S. Singh, R. Misra and R. Pratap, *RSC Adv.*, 2014, **4**, 56779.
37 D. Singhal, I. Althagafi, A. Kumar, S. Yadav, A. K. Prasad and R. Pratap, *New J. Chem.*, 2020, **44**, 12019.
38 A. Jauhari, *et al.*, *Mol. Neurobiol.*, 2018, **55**, 936.
39 (*a*) A. Pandey, *et al.*, *Toxicol. Res.*, 2015, **4**, 1578; (*b*) Z. Ruzi, A. Buronov, L. Nie, A. Nasrullaev, Z. Murtazaeva, R. Kuryazov, J. Zhao, T. Efferth, H. Akber and K. Bozorov, *Int. J. Mol. Sci.*, 2025, **26**(17), 8528; (*c*) M. M. Fouad, H. A. Ghabbour, I. A. Shehata and M. B. El-Ashmawy, *Bioorg. Chem.*, 2024, **148**, 107401; (*d*) E. S. M. Elsenbawy, Z. S. Alshehri, N. A. Babteen, A. A.-H. Abdel-Rahman, M. A. El-Manawaty, E. S. Nossier, R. K. Arafa and N. A. Hassan, *Molecules*, 2024, **29**(5), 1067; (*e*) A. Rogova, I. A. Gorbunova, T. E. Karpov, R. Y. Sidorov, A. E. Rubtsov, D. A. Shipilovskikh, A. R. Muslimov, M. V. Zyuzin, A. S. Timin and S. A. Shipilovskikh, *Eur. J. Med. Chem.*,

2023, **254**, 115325; (*f*) R. Vasamsetti, N. B. Gatchakayala, P. V. Kumar, C. Praveen, S. V. G. V. A. Prasad and B. Madhav, *Results Chem.*, 2024, 101823.

40 (*a*) J. H. Park, Y. Liu, M. A. Lemmon and R. Radhakrishnan, *Biochem. J.*, 2012, **448**, 417; (*b*) S. Bhardwaj and A. K. Yadav, *J. Neuro Oncol.*, 2025, **171**, 47–63.

41 E. A. Sobh, M. A. Dahab, E. B. Elkaeed, A. A. Alsfouk, I. M. Ibrahim, A. M. Metwaly and I. H. Eissa, *J. Enzyme Inhib. Med. Chem.*, 2023, **38**, 2220579.

42 P. Limpachayaporn, S. Nuchpun, J. Sirirak, P. Charoensuksai, P. Wongprayoon, N. Chuaypen, P. Tangkijvanich and A. Suksamrarn, *Bioorg. Med. Chem.*, 2022, **74**, 117048.

43 D. K. Yadav, S. Kumar, Saloni, S. Misra, L. Yadav, M. Teli, P. Sharma, S. Chaudhary, N. Kumar, E. H. Choi, H. S. Kim and M. H. Kim, *Sci. Rep.*, 2018, **8**, 4777.